

Accurate water properties from an efficient ab-initio method

Subrata Jana,^{1,*} Lucian A. Constantin,^{2,†} and Prasanjit Samal^{1,‡}

¹*School of Physical Sciences, National Institute of Science Education and Research, HBNI, Bhubaneswar 752050, India*

²*Center for Biomolecular Nanotechnologies @UNILE,
Istituto Italiano di Tecnologia, Via Barsanti, I-73010 Arnesano, Italy*

(Dated: October 1, 2019)

Accurate prediction of the water properties from a low-cost ab-initio method still a foremost problem for chemists and physicist. Though density functional approaches starting from semilocal to hybrid functionals are tested, those are not efficiently performed for all the properties together, especially, considering energies, conformational ranking, structural and dynamics of water. Also, the inclusion of the long-range van der Waals (vdW) interaction does not improve the ordering stability of isomer. However, relying on the simple revision of the Tao-Mo (revTM) semilocal meta-generalized gradient approximations, we demonstrate that all properties of the water can be accurately predicted. A consistent improvement over several popular ab-initio methods is achieved, indicating the accuracy of this method for describing hydrogen bonding of water.

I. INTRODUCTION

Density functional theory (DFT)¹ is the *de-facto* standard method to calculate the electronic properties of molecules, solids, and liquids. DFT, which relies on the accuracy of the different levels of exchange-correlation (xc) approximations^{2–44}, performs remarkably for different interactions with or without weak dispersion correction^{26,45–67}. In spite of its successes, describing the order of stability and the energetics of low-lying water cluster ((H₂O)_n) isomer (e.g. for the hexamer ($n = 6$) and pentamer ($n = 5$)), and different ice phases are great challenges for semilocal DFT⁶⁸. There have been several research works devoted, mainly on the accuracy of a particular theoretical method for liquid water and ice phases^{69–74}. Experimentally, also, a lot of attention has been paid on the binding nature and conformational ranking of different low-lying water isomer and ice phases^{68,70,75–77}.

Physically, the interactive nature of the water is hydrogen (H) bonded. In the H-bond, a non-negligible electronic charge overlap happens between the bonding constituents, whose interaction nature is neither fully density overlap (like covalent bonds) nor weak van-der-Waals (vdW) forces. In H-bonding both the charge transfer (CT) and dipole interactions (DI) effects are observed⁷⁸. The H-bond holds the water in its liquid, gas or crystal ice form, and the H-bonding potential energy surfaces can be modelled using several methods based on the properties of the electronic density, such as the theory of atoms in molecules^{79–81}, and the noncovalent interaction index^{82,83}.

Based on several experimental and theoretical confirmations, there exist five to eight low-lying energy isomer of the water hexamer in nature^{84–86}. Moreover, isomer for the trimer, tetramer, pentamer and higher order cluster are also found^{87–89}. Besides, several phases of ice have been also found^{90–92}. However, the correct prediction of the ordering, stability and most preferred structure of the water isomer and ice phases, is a difficult problem for theoretical methods^{68,93,94}. In this re-

gard, several ab-initio studies have been performed on the level of accurate wavefunction (Møller-Plesset perturbation theory (MP2) and quasi-perturbative connected triple excitations (CCSD(T)))^{68,95–97}, diffusion Monte Carlo (DMC)⁹³ and density functional^{68,71,93,98}. The stable isomer of the water hexamer⁹⁵ are the prism, cage, book1, book2, bag, cyclic-chair, cyclic-boat2, and cyclic-boat2, and those are utilized for benchmark performance of different wavefunction and density functional based approaches^{68,93,95–97}. Though the CCSD(T), MP2 and DMC predict correctly the order of stability of these water isomer, their computational costs are expensive. Hence, the most preferred method is the density functional semilocal approach.

Regarding the performance of semilocal DFT for water, different xc functionals behave differently to describe the H-bond, which is relatively weaker than the covalent interaction but stronger than the pure dispersion bond, being comparable in magnitude with the CT and DI interactions. Moreover, in a system like water, there is a competition between the covalent, H-bond and dispersion bonds⁶⁸ and a good semilocal or vdW corrected functional must be able to describe all these bonds in order to perform quite conventionally for water.

In several previous studies, the bare semilocal xc functionals and long-range corrected hybrids, together with their dispersion corrected versions have been tested for the water hexamer^{71,93,94,96}. Considering the recent progress on semilocal DFT, it was shown that the Strongly Constrained and Appropriately Normed Semilocal Density Functional (SCAN)³⁷ functional performs quite well for the different phases of water, isomer and ice, being also very accurate for the polarizability, dipole moments and diffusion coefficient⁷¹. It can accurately describe the short and intermediate range of non-covalent interactions, being capable to capture the H-bonding nature of the water. However, SCAN overestimates the total energies of the water hexamer isomer and cluster, comparing with the MP2^{93–97}, and CCSD(T) results⁸⁶. Note that the MP2 and CCSD(T) within complete basis set limit (CBS) methods are considered as the state-of-

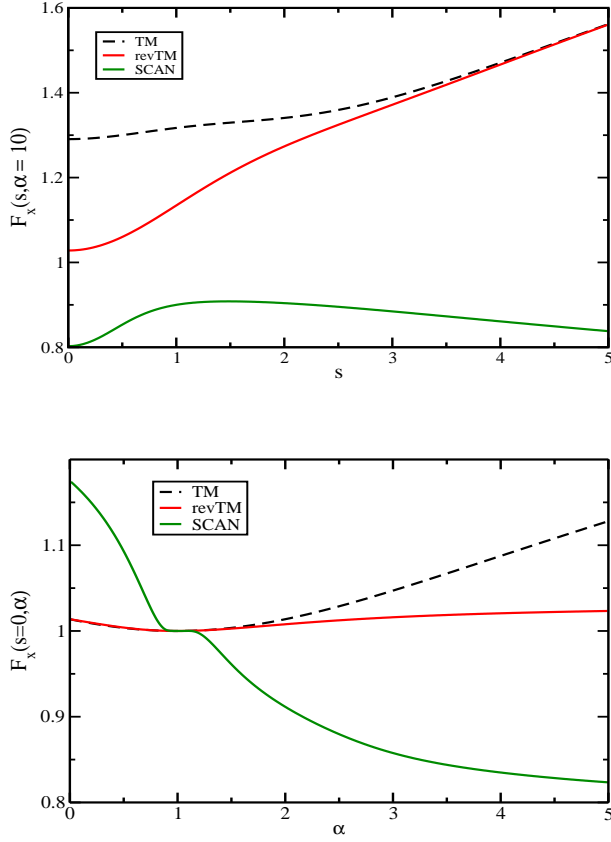


FIG. 1. Exchange enhancement factor $F_x(s, \alpha)$ of TM, revTM, and SCAN meta-GGA functionals as a function of the reduced gradient s (upper panel) and of the Pauli kinetic energy enhancement factor α (lower panel).

art for the reference energies of water isomer, and they are using for benchmarking xc functionals^{95–97}.

In this paper, we investigate the behavior of the recently proposed meta-generalized gradient approximations (meta-GGAs) for the relative energies of the different low-lying water isomer and cluster, conformational ranking, vibrational frequencies, and properties of ice phases. Keeping in mind that there are several previous studies⁶⁸, we consider only selected semilocal xc functionals in this work. We restrict ourselves only on the level of semilocal approximations because of their simplicity and quick output for studying large water cluster. We are mainly focusing on the performance of the recently proposed Tao-Mo (TM)³⁸ meta-GGA and its revised form (revTM)⁴². For comparison, the PBE and SCAN results are also included. The present paper is arranged as follows: In the next section, we describe the methods and showing a brief outline of the TM and revTM functionals. Following this, we discuss the obtained results and comparison of different functionals. We summarize and conclude our results lastly.

II. THEORY

Our starting point is the construction of the TM³⁸ and revTM⁴² functionals. In DFT, the xc energy functional is defined as,

$$E_{xc} = \int d\mathbf{r} \rho(\mathbf{r}) \epsilon_{xc}(\mathbf{r}), \quad (1)$$

where ρ is the electron density and $\epsilon_{xc}(\mathbf{r})$ is the xc energy per particle. The meta-GGA exchange functional is,

$$E_x = \int d\mathbf{r} \rho(\mathbf{r}) \epsilon_x^{unif}(\mathbf{r}) F_x(\rho, \nabla \rho, \tau^{KS}), \quad (2)$$

where τ^{KS} is the KS kinetic energy density, F_x is the exchange enhancement factor, and ϵ_x^{unif} is the exchange energy per particle of the uniform electron gas. In Ref.⁴², the construction of the revTM is discussed in detail along with the TM functional. Here, we only focus on the key differences of the two functionals. The TM exchange enhancement factor³⁸ is given by

$$F_x^{TM} = w F_x^{DME} + (1 - w) F_x^{sc}, \quad (3)$$

where w is a weighting factor, F_x^{DME} is the density matrix expansion (DME) based semilocal exchange enhancement factor and F_x^{sc} is the enhancement factor of the fourth-order gradient expansion (GE4) exchange energy. The DME part is accurate for the localized systems such as atoms and molecules, whereas the GE4 is accurate for slowly varying solid-state systems. See Refs.^{38,42} for details.

In the revTM functional, the DME part remains unaltered, whereas the slightly different form of the F_x^{sc} is proposed. The F_x^{sc} of TM functional is given by

$$F_x^{sc} = \{1 + 10[(10/81 + 50p/729)p + 146\tilde{q}^2/2025 - (73\tilde{q}/405)[3\tau_W/(5\tau)](1 - \tau_W/\tau)]\}^{1/10}, \quad (4)$$

where $p = s^2$ with $s = |\nabla \rho|/[2(3\pi^2)^{1/3}\rho^{4/3}]$ being the reduced gradient, and $\tilde{q} = (9/20)(\alpha - 1) + 2p/3$ is finite near the nucleus (where $\alpha \approx 0$ and $s \approx 0.4$) and otherwise mimics the reduced Laplacian of the density (a.i. $q = |\nabla^2 \rho|/[4(3\pi^2)^{2/3}\rho^{5/3}]$) outside of the nuclear region. Here $\alpha = \frac{\tau - \tau_W}{\tau_{unif}}$ is the Pauli kinetic energy enhancement factor used as a meta-GGA ingredient, being also an iso-orbital indicator, $\tau_W = \frac{|\nabla \rho|^2}{8\rho}$ is the von Weizsäcker kinetic energy density, and τ_{unif} is the kinetic energy density of the uniform electron gas. The difference of the TM and revTM in the exchange part comes from the construction of the \tilde{q} . Instead of the above defined \tilde{q} as used in the TM functional, in revTM a slightly modified $\tilde{q}_b = \frac{9(\alpha-1)}{20[1+b\alpha(\alpha-1)]^{1/2}} + \frac{2p}{3}$ is considered with $b = 0.40$ ⁹⁹. Due to this modification, the revTM functional behaves differently in the region $\alpha \gg 1$ (recognized as the overlapping closed shells⁵⁴) and $s \approx 0$. The $\alpha \gg 1$ region, where $F_x^{revTM} \leq F_x^{TM}$ by construction, is found in the bonds of the H-bond, CT, and DI complexes.

In Fig. 1 we show a comparison of the TM, revTM, and SCAN meta-GGA enhancement factors. In the upper panel we plot $F_x(s, \alpha = 10)$ versus s . The difference between TM and revTM is decreasing when s increases, being maximum at $s = 0$, and vanishing at $s \approx 3.5$. However, both TM and revTM exchange enhancement factors increase monotonically, enhancing over the Local Density Approximation (LDA) (note that $F_x^{LDA} = 1$). Oppositely, SCAN shows important de-enhancement ($F_x^{SCAN} \leq 1$), with a hill-like structure. Large values of α , such as $\alpha = 10$, are present in non-covalent bonds and in the tail of the density due to the degenerate valence shells.

In the lower panel of Fig. 1, we plot $F_x(s = 0, \alpha)$ versus α . The revTM remains almost steady for the whole range of the α , whereas the TM monotonically increases from $\alpha \geq 1$, and SCAN decreases. At $\alpha = 0$, TM and revTM are close to LDA, while SCAN approaches its maximum value of 1.174³⁷. At $\alpha = 1$, all functionals recover, by construction, the LDA behavior. Note that always $s = 0$ in the middle of any bond, while $\alpha \approx 1$ for strong bonds (e.g. covalent bonds), $\alpha \geq 1$ for weak bonds (e.g. non-covalent bonds), and $\alpha \approx 0$ in the bonds where the valence atomic shells are non-degenerate (e.g. H_2 , Be_2).

The TM correlation functional is just a modified TPSS correlation with an improved performance in the low-density limit³⁸. The $\beta = 0.066725$ parameter used in the TM functional is same as TPSS and PBE, representing the second-order coefficient of the correlation energy gradient expansion in the high-density limit. But, in the revTM β is changed to $\beta^{revTPSS}(r_s) = 0.066725(1 + 0.1r_s)/(1 + 0.1778r_s)$, which is the correct, density-dependent second-order coefficient. Here r_s is the bulk parameter (also called Wigner-Seitz radius). Apart from this modification, the revTM keeps all the good properties of the TM correlation energy functional. Note that the change in the correlation part bit improves the atomization energies of molecules⁴².

In order to better understand and quantify the differences between the considered functionals, we report in Table I a comparison between PBE, SCAN, TM and revTM for the H-bond (HB6 test set¹⁰⁰), dipole-dipole interaction (DI6 test set¹⁰⁰), and charge transfer interaction (CT7 test set¹⁰⁰). All these tests (HB6, DI6, and CT7) are representative, well-known and widely used. For all the systems, with the exception of NH_3-ClF charge-transfer complex, the revTM gives smaller deviations than TM, mainly due to the less exchange enhancement shown in Fig. 1. Moreover, for all the tests, revTM improves over TM, showing the best performance, and implicitly the best overall error (TMAE=1.09 kcal/mol).

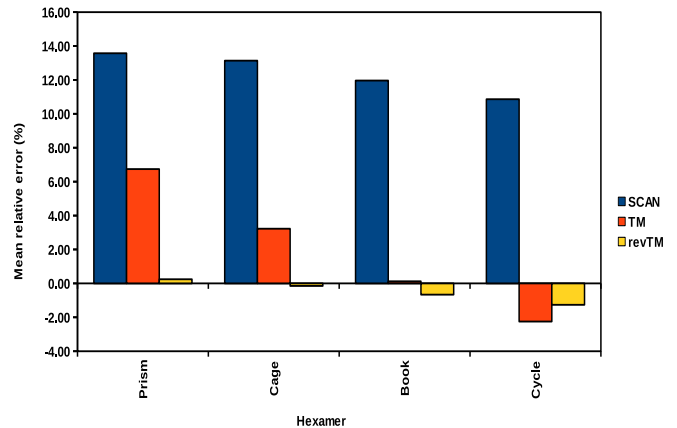


FIG. 2. Shown is the percentage deviation in binding energy per monomer, for different meta-GGA functionals compared to the MP2 reference, of the four water hexamer shown in Table II.

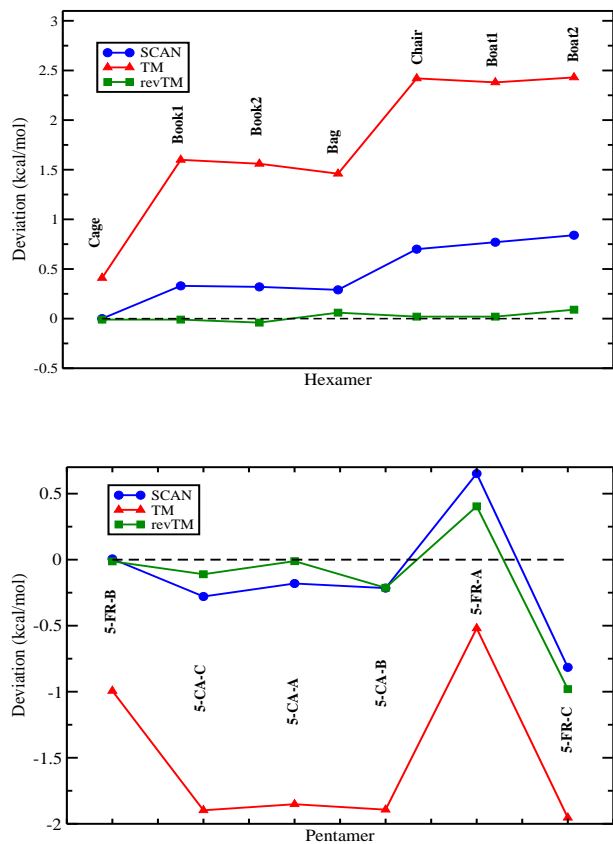


FIG. 3. Deviation (result - reference) of the different functionals for the water hexamer of Table III (upper panel) and water pentamer of Table IV (lower panel). Only meta-GGA functionals are considered here.

TABLE I. The reference values of the interaction energies, and the deviations (result - reference) obtained from several xc functionals, for the HB6^{57,100}, DI6^{57,100} and CT7^{57,100} representative test sets. The 6-311++G(3df,3pd) basis set within NWCHEM code is used⁴². All values are in kcal/mol. We also report the mean error (ME) and mean absolute error (MAE) for each test, and the overall total ME (TME), and total MAE (TMAE). Best (T)MAE is in bold style.

Complex	Ref.	PBE	SCAN	TM	revTM
HB6 (kcal/mol)					
NH ₃ -NH ₃	3.1	0.0	0.3	0.0	-0.2
HF-HF	4.6	0.3	1.1	0.4	0.1
H ₂ O-H ₂ O	5.0	0.2	0.7	0.1	0.0
NH ₃ -H ₂ O	6.4	0.5	0.6	0.1	0.1
HCONH ₂ -HCONH ₂	14.9	-0.6	1.1	-0.2	-0.7
HCOOH-HCOOH	16.1	0.3	1.8	0.4	0.0
ME		0.1	0.9	0.1	-0.1
MAE		0.3	0.9	0.2	0.2
DI6 (kcal/mol)					
H ₂ S-H ₂ S	1.7	0.0	-1.7	0.0	-0.2
HCl-HCl	2	-0.1	0.6	0.1	-0.1
HCl-H ₂ S	3.4	-0.7	0.2	0.5	0.4
CH ₃ Cl-HCl	3.5	0.1	1.7	0.5	-0.1
HCN-CH ₃ SH	3.6	0.1	0.8	0.2	-0.2
CH ₃ SH-HCl	4.2	-1.4	2.0	1.7	1.2
ME		-0.3	0.6	0.5	0.2
MAE		0.4	1.2	0.5	0.4
CT7 (kcal/mol)					
C ₂ H ₄ -F ₂	1.06	2.14	1.84	2.14	1.84
NH ₃ -F ₂	1.81	3.49	2.59	3.19	2.89
C ₂ H ₂ -ClF	3.81	2.29	3.49	2.99	2.59
HCN-ClF	4.86	0.94	0.64	1.24	0.94
NH ₃ -Cl ₂	4.88	3.02	2.52	3.02	2.82
H ₂ O-ClF	5.36	1.84	2.34	2.44	2.14
NH ₃ -ClF	10.62	6.28	6.48	5.78	5.88
ME		2.86	2.84	2.97	2.73
MAE		2.86	2.84	2.97	2.73
TME		0.88	1.46	1.20	0.93
TMAE		1.19	1.65	1.22	1.09

III. RESULTS AND DISCUSSIONS

A. Water isomer

In Table II, we present the binding energies per monomer of four low-lying isomer of the water hexamer (prism, cage, book and cycle), obtained from the PBE, SCAN, TM and revTM functionals, using the MP2 optimized geometries⁹³. For the reference energy benchmarks we consider the MP2^{86,93,94}, CCSD(T)/CBS⁹⁵, and DMC⁹³ values. Note that, the MP2 is the standard procedure for benchmarking the water hexamer as it is used in different works^{86,93,94,96,97,107–109}. Considering earlier attempts, it was shown that GGA (PBE) and GGA with vdW correction (GGA+vdW) functionals predict wrong energy ordering of the water hexamer⁹³, whereas, SCAN meta-GGA gives the correct ordering⁹⁸. In Table II, it is shown that along with SCAN, the TM and revTM functionals also predict the correct ordering and stability (prism > cage > book > cycle) of these water hexamer. Moreover, the obtained energies from revTM functional agree closely with that of the MP2,

DMC, and CCSD(T) results. On the other hand, the TM functional is close to the CCSD(T) results, while SCAN functional shows the most overestimation tendency within the considered functionals. The remarkable performance of the revTM functional is shown in Fig. 2, where we also plot the relative errors (in %) of SCAN, TM and revTM meta-GGAs.

Next we focus on the relative stability of different low-lying isomer of the water hexamer, with respect to the prism structure, which is the most stable. Our results are summarized in Table III. Note that the prediction of accurate relative energies is still a long-standing problem. Very recently, it was shown that the SCAN meta-GGA performs efficiently and predicts the correct order of stability, but the relative binding energies of each hexamer with respect to the prism structure, are overestimated^{71,72,98,110,111}. In our present study, we also found a similar tendency for the SCAN functional. However, from Table III, we observe that the revTM functional performs remarkably and getting the absolute binding energies in very good agreement with the CCSD(T)/CBS reference. The revTM functional obtains the smallest mean absolute error

TABLE II. Binding energies per monomer (in meV/H₂O) of four water hexamer obtained from different functionals. The reference MP2, CCSD(T) and DMC reference values are taken from Refs.⁹³. The MP2 optimized geometries⁹³ are considered for single-point energy calculations. The aug-cc-pVTZ basis set is used. The most stable structure is in bold style.

Methods	Prism	Cage	Book	Cycle
MP2	332.3	331.9	330.2	324.1
DMC	331.9	329.5	327.8	320.1
CCSD(T)	347.6	345.5	338.9	332.5
PBE	336.1	338.1	344.0	341.7
$E_{PBE}-E_{MP2}$	3.8	6.2	13.8	17.6
$E_{PBE}-E_{DMC}$	4.2	8.6	16.1	21.6
$E_{PBE}-E_{CCSD(T)}$	-11.5	-7.4	5.1	9.2
SCAN	377.4	375.5	369.7	359.3
$E_{SCAN}-E_{MP2}$	45.0	43.6	39.5	35.2
$E_{SCAN}-E_{DMC}$	45.5	46.0	41.9	39.2
$E_{SCAN}-E_{CCSD(T)}$	29.8	30.0	30.8	26.8
TM	354.7	342.6	330.6	316.8
$E_{TM}-E_{MP2}$	22.4	10.7	0.34	-7.3
$E_{TM}-E_{DMC}$	22.8	13.1	2.8	-3.3
$E_{TM}-E_{CCSD(T)}$	7.1	-2.9	-8.3	-15.7
revTM	333.1	331.4	328.0	320.0
$E_{revTM}-E_{MP2}$	0.8	-0.5	-2.2	-4.1
$E_{revTM}-E_{DMC}$	1.2	1.9	0.2	-0.1
$E_{revTM}-E_{CCSD(T)}$	-14.5	-14.1	-10.9	-12.5

TABLE III. Relative binding energies (with respect to the prism structure) for different low-lying energy isomer of the water hexamer. The reference values are from high-level wavefunction calculations (CCSD(T)/CBS of Ref.⁹⁵). The MP2/aug-cc-pVTZ level geometries⁹⁷, and the aug-cc-pVTZ basis set are used. All results are in kcal/mol. Best calculated values are in bold style.

Methods	Cage	Book1	Book2	Bag	Chair	Boat1	Boat2	ME	MAE
Ref.	0.25	0.72	1.02	1.62	1.80	2.79	2.85	—	—
PBE	-0.27	-1.07	-0.81	-0.06	-0.76	0.29	0.46	-1.90	1.90
SCAN	0.25	1.05	1.34	1.91	2.50	3.56	3.69	0.46	0.46
TM	0.66	2.32	2.58	3.08	4.22	5.17	5.28	1.75	1.75
revTM	0.24	0.71	0.98	1.68	1.82	2.81	2.94	0.02	0.03

(MAE=0.03 kcal/mol), that is an order of magnitude better than SCAN (MAE=0.46 kcal/mol). Whereas, the TM functional tends to overestimate the binding energies (MAE=1.75 kcal/mol), but still gives the correct ordering between the hexamer. In the upper panel of Fig 3, we plot the deviations (result - reference) of meta-GGA functionals, for all considered isomer, showing that the revTM functional is almost exact.

To stress on the remarkable performance of revTM functional, in Table IV, we also consider the relative binding energies of the low-lying water isomer for the tetramer ($n = 4$) and pentamer ($n = 5$), and compare those with the CCSD(T)/CBS level theory¹⁰¹. For the pentamer structures, the cycle (5-CYC) is the most stable structure. In this case also, the revTM functional performs remarkable well and reproduce the correct ordering, with exception of the 5-FR-C pentamer where all functionals wrongly predict it to be before the 5-FR-A isomer. The SCAN functional is the second-best performer, while the TM functional fails not only to show the correct order, but also gives 5-CA-C as the most stable structure, instead of 5-CYC. This is an important shortcoming of the TM meta-GGA which revTM functional is able to solve it. Finally, in the lower panel of Fig. 3, we also plot the

deviations in the relative binding energies of these water pentamer. From this plot one can also observe that the revTM functional is performing best compared to the others.

In the simpler case of the tetramer, all functionals show the correct order between the 4-S₄, 4-Ci, and 4-Py isomer. However, the relative binding energies between the 4-Ci and 4-Py are: 2.7 kcal/mol for reference, 4.27 kcal/mol for PBE, 2.84 kcal/mol for SCAN, 1.58 kcal/mol for TM, and 2.78 kcal/mol for revTM.

B. Water cluster

Let us now consider the small water cluster (with most stable structure) to assess the quality of the different functionals. The results of the dimer, trimer, tetramer, and pentamer are presented in Table V. These small water cluster have been used to test the performance of several density functionals⁶⁹. However, We observe the remarkable accuracy of the revTM functional with the smallest overall error (MAE=2.4 meV/H₂O), followed by TM (MAE=5.8 meV/H₂O), and PBE (MAE=9.7 meV/H₂O), while SCAN strongly overestimates the dis-

TABLE IV. Comparison of relative binding energies with respect to the most stable structure (a.i. 4-S₄ for tetramer and 5-CYC for pentamer) of water tetramer and pentamer low-lying energy isomer¹⁰¹, using different methods. The CCSD(T)/CBS reference values are taken from¹⁰¹. The RI-MP2/aVDZ optimized coordinates¹⁰¹ and the aug-cc-pVTZ basis set are used. All results are in kcal/mol. Best calculated values are in bold style.

	4-Ci	4-Py	5-FR-B	5-CA-C	5-CA-A	5-CA-B	5-FR-A	5-FR-C
Ref.	0.85	3.55	1.14	1.32	1.47	2.19	2.88	3.57
PBE	0.89	5.16	2.42	3.32	3.65	4.07	4.62	3.95
SCAN	0.95	3.79	1.15	1.04	1.29	1.97	3.53	2.75
TM	0.89	2.47	0.15	-0.58	-0.38	0.30	2.36	1.62
revTM	0.88	3.66	1.13	1.21	1.46	1.98	3.28	2.59

TABLE V. Comparison of different functionals for four different stable water cluster ((H₂O)_n, with $n = 2$ to 5). The MP2/CBS reference dissociation energies per monomer (in meV/H₂O) are taken from⁶⁹. The single point energy calculations are done with MP2/aug-cc-pVTZ level geometries⁶⁹. In parentheses we report the percentage deviation from the dissociation energy of the dimer. The aug-cc-pVTZ basis set is used. Best calculated values are in bold style.

Methods	Dimer	Trimer	Tetramer	Pentamer	ME	MAE
MP2	215.8	228.5 (5.9)	299.9 (38.9)	314.4 (45.7)	—	—
PBE	219.2	231.1 (5.4)	314.3 (43.4)	332.7 (51.8)	9.7	9.7
SCAN	235.1	256.6 (9.1)	335.9 (42.8)	350.8 (49.2)	30.0	30.0
TM	217.2	241.1 (11.0)	306.5 (41.1)	317.0 (46.0)	5.8	5.8
revTM	209.4	228.5 (9.1)	299.0 (42.8)	312.2 (49.1)	-2.3	2.4

sociation energies giving MAE=30.0 meV/H₂O. To incorporate the H bond strength, in Table V we also report, for each functional, the percentage deviation in dissociation energy per monomer, of the trimer, tetramer, and pentamer with respect to the dimer. From these results we observe that all the functionals perform equivalently. However, the revTM functional is a bit closer to the SCAN functional.

C. Performance for the WATER27 subset

The remarkable accuracy of the revTM functional is also proved from Table VI, where we consider the binding energies of the 27 neutral, positively, and negatively charged water cluster (WATER27) from the well known GMTKN55 test set⁶³. This test set consists of 10 neutral (H₂O)_n structures (with $2 \leq n \leq 8$), 4 isomer of (H₂O)₂₀, 5 protonated water cluster of the form H₃O⁺(H₂O)_n (with $1 \leq n \leq 6$), 7 deprotonated cluster of the form OH⁻(H₂O)_n (with $1 \leq n \leq 6$), and 1 mixed hydroxonium-hydroxide zwitterion. Results of Table VI indicate the astonishing performances of both TM and revTM with overall errors smaller than 1.5 kcal/mol, followed by PBE (TMAE=2.35 kcal/mol). In this case, the SCAN functional deviates most (with TMAE=7.4 kcal/mol), showing a quite modest performance especially for the isomer of (H₂O)₂₀.

D. Structural and vibrational properties

In Table VII we report the bond length, bond angle, dipole moment and static polarizability of the water monomer. We observe that TM and revTM functionals

perform similarly, being slightly better than PBE, but noticeably worse than SCAN meta-GGA. Both TM and revTM overestimate the bond length and static polarizability, and underestimate the bond angle and dipole moment

To assess the functionals for the harmonic vibrational frequencies of the water, we consider several water cluster (H₂O)_n ($n = 1 - 5$), and isomer ($n = 6$). The full results are provided in Ref.¹⁰⁴, and here we summarize them in Table VIII and Fig 4. As reference, we considered the CCSD(T) results from Refs.^{101,112,113}. For the water monomer, we obtain the same trend as in Table VII, with SCAN being remarkably accurate (MARE= 0.7%), while TM (MARE=2.8%) and revTM (MARE=2.8%) being slightly better than PBE (MARE=3.6%), which gives the worse performance. On the other hand, for all the other systems, from dimer to hexamer, SCAN works in line with, and sometimes worse than PBE, giving large errors ($6.1 \% \leq \text{MARE} \leq 15.8\%$). These results are also in agreement with Tables II and V, where SCAN gives significant overestimation of the binding energies of the water cluster. Finally, we observe that TM and revTM perform accurately for the harmonic vibrational frequencies, being able to describe all the systems within MARE≤5.1 %. They are very good especially for lower frequencies $\nu < 1000 \text{ cm}^{-1}$, whereas SCAN is the slightly better functional for higher frequencies ($\nu > 1000 \text{ cm}^{-1}$). Note that PBE functional overestimates the vibrational frequencies for $\nu < 1000 \text{ cm}^{-1}$ and underestimates the same for $\nu > 1000 \text{ cm}^{-1}$.

TABLE VI. The reference values and the deviations (result - reference) obtained from xc functionals, for the WATER27 test set⁶³. The CCSD(T)-F12/CBS reference values are taken from Ref.¹⁰². The def2-QZVPD basis set is used. All values are in kcal/mol. Best MAE are in bold style.

Complex	Ref.	PBE	SCAN	TM	revTM
neutral (kcal/mol)					
(H ₂ O) ₂	4.974	0.082	0.420	0.010	-0.167
(H ₂ O) ₃ cyclic	15.708	0.262	1.903	0.850	0.008
(H ₂ O) ₄ cyclic	27.353	1.519	3.333	0.720	0.041
(H ₂ O) ₅ cyclic	35.879	2.299	4.211	0.459	-0.117
(H ₂ O) ₆ prism	45.988	0.096	5.351	2.351	-0.531
(H ₂ O) ₆ cage	45.733	0.697	5.412	2.029	-0.432
(H ₂ O) ₆ book	45.292	2.016	5.269	1.052	-0.291
(H ₂ O) ₆ cyclic	44.296	2.765	4.990	0.297	-0.306
(H ₂ O) ₈ cube (D _{2d})	72.490	1.492	8.215	2.427	-0.886
(H ₂ O) ₈ cube (S ₄)	72.454	1.515	8.262	2.426	-0.875
(H ₂ O) ₂₀ dodecahedron	197.804	9.163	21.009	1.101	-3.450
(H ₂ O) ₂₀ fused cubes	207.534	-2.506	20.763	6.356	-5.775
(H ₂ O) ₂₀ face-sharing	207.763	-0.464	20.259	4.029	-6.331
(H ₂ O) ₂₀ edge-sharing	209.081	1.415	20.687	3.835	-5.417
ME		1.454	9.292	1.996	-1.752
MAE		1.878	9.292	1.996	1.759
protonated (kcal/mol)					
(H ₃ O) ⁺ (H ₂ O)	33.738	3.169	3.040	0.404	0.525
(H ₃ O) ⁺ (H ₂ O) ₂	57.114	3.262	4.037	0.171	0.284
(H ₃ O) ⁺ (H ₂ O) ₃	76.755	2.924	4.142	-0.105	-0.110
(H ₃ O) ⁺ (H ₂ O) ₆ (3D)	117.683	3.142	7.246	0.905	-0.873
(H ₃ O) ⁺ (H ₂ O) ₆ (2D)	114.819	4.312	6.580	-0.367	-1.052
ME		3.362	5.009	0.201	-0.245
MAE		3.362	5.009	0.390	0.569
deprotonated (kcal/mol)					
OH ⁻ (H ₂ O)	26.687	2.165	2.797	0.187	0.137
OH ⁻ (H ₂ O) ₂	48.688	1.983	3.785	0.005	-0.128
OH ⁻ (H ₂ O) ₃	67.525	1.837	4.470	-0.068	-0.416
OH ⁻ (H ₂ O) ₄ (C ₄)	84.351	-0.426	5.035	0.799	-1.146
OH ⁻ (H ₂ O) ₄ (C _s)	85.015	0.458	6.243	1.457	-0.682
OH ⁻ (H ₂ O) ₅	100.782	-0.995	7.138	2.663	-0.705
OH ⁻ (H ₂ O) ₆	115.672	-0.526	8.485	2.719	-0.978
ME		0.643	5.422	1.109	-0.560
MAE		1.199	5.422	1.128	0.599
mixed (kcal/mol)					
(H ₂ O) ₈ cube (S ₄) - H ₃ O ⁺ (H ₂ O) ₆ OH ⁻	29.605	-12.003	-8.060	-0.963	-3.724
ME		-12.003	-8.060	-0.963	-3.724
MAE		12.003	8.060	0.963	3.724
TME		1.10	6.85	1.32	-1.24
TMAE		2.35	<u>7.44</u>	1.44	1.31

TABLE VII. Bond lengths (Å), bond angle (degrees), dipole moment (Debye), and static polarizability (a.u.) of the water monomer. The experimental reference values are taken from Refs.^{78,103}. The aug-cc-pVTZ basis set is used.

	Expt.	PBE	SCAN	TM	revTM
$R(O-H)$	0.957	0.970	0.961	0.969	0.969
$\angle HOH$	104.5	104.2	104.4	103.9	104.0
μ	1.855	1.804	1.840	1.794	1.798
α	9.92	10.33	9.81	10.29	10.28

E. Performance for ice

The ab-initio studies of ice phases are also quite important. Several experimental structures suggested that

15 ice phases exist^{92,105,114,115}. Most of them are constructed from the proton disordered phases, having complex structures. However, only seven ice phases, the ice Ih and six other proton ordered phases (IX, II, XIII, XIV, XV, and VIII) are considered to perform benchmark calculations for the semilocal, non-local and vdW corrected functionals^{92,105}. Among all these phases the ice Ih is the most stable structure. In this subsection we will report the performance of the different density functional approaches for the sublimation or lattice energies of the ice and zero pressure volumes.

The sublimation energy per H₂O of ice phases, represents the energy per monomer required to change the ice

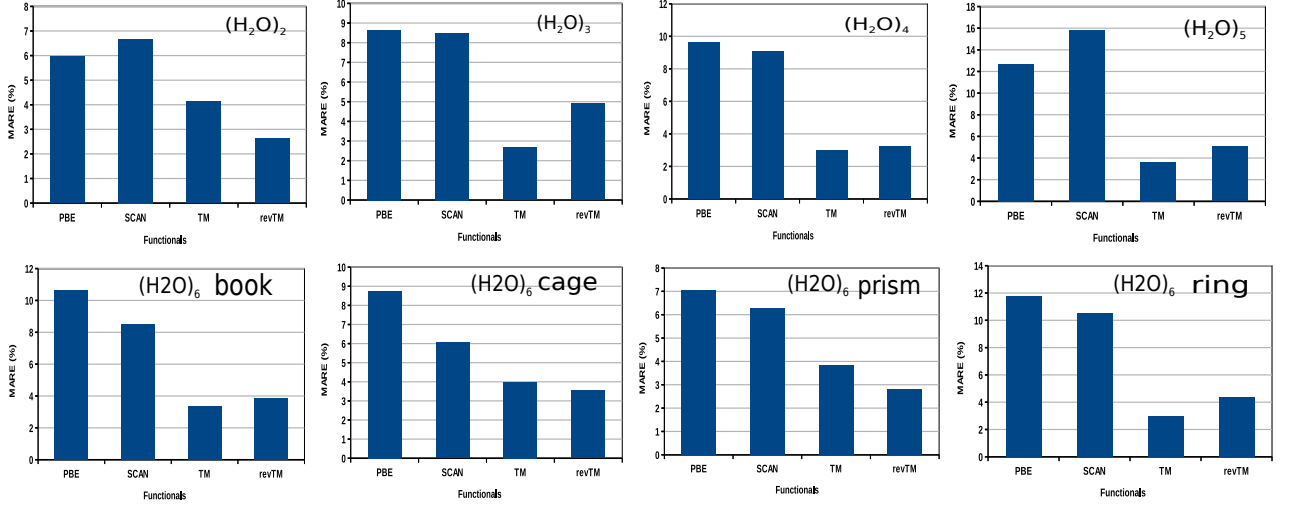


FIG. 4. MAREs of vibrational frequencies obtained from different xc functionals, for the water cluster and isomer of Table VIII.

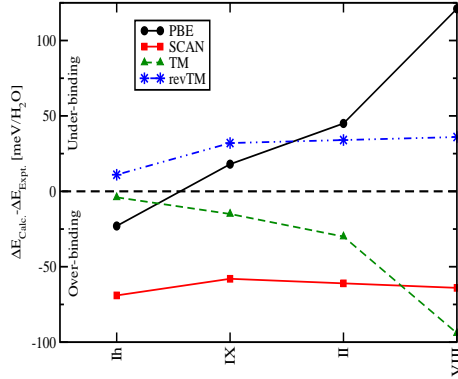


FIG. 5. Deviations in the formation energies of several ice phases, obtained from different xc functionals. (See Table IX.)

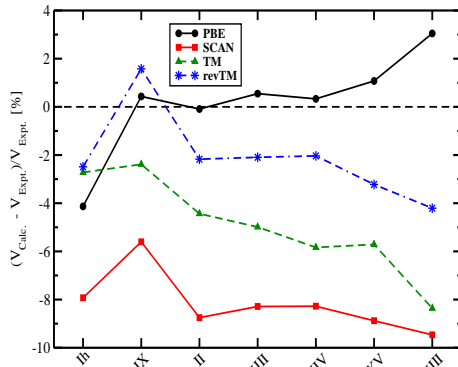


FIG. 6. Shown is the relative differences in the volume of ice as calculated using different methods. (See Table X.)

TABLE VIII. Mean absolute relative error (MARE) (in %) of harmonic vibrational frequencies for water cluster and hexamer isomer, using different methods. All values are in cm^{-1} and calculated with an aug-cc-pVTZ basis set. Details of reference and individual values are given in Ref.¹⁰⁴.

	PBE	SCAN	TM	revTM
H_2O	3.6	0.7	2.8	2.8
$(\text{H}_2\text{O})_2$	6.0	<u>6.7</u>	4.1	2.6
$(\text{H}_2\text{O})_3$	<u>8.6</u>	8.5	2.7	4.9
$(\text{H}_2\text{O})_4$	<u>9.7</u>	9.1	3.0	3.2
$(\text{H}_2\text{O})_5$	12.7	<u>15.8</u>	3.6	5.1
$(\text{H}_2\text{O})_6$ -book	<u>10.7</u>	8.5	3.3	3.9
$(\text{H}_2\text{O})_6$ -cage	<u>8.8</u>	6.1	4.0	3.5
$(\text{H}_2\text{O})_6$ -prism	<u>7.1</u>	6.3	3.8	2.8
$(\text{H}_2\text{O})_6$ -ring	<u>11.8</u>	10.5	3.0	4.3

into gas phase, and is defined as,

$$\Delta E = (E^{Ice} - N \times E^{H_2O})/N, \quad (5)$$

where E^{Ice} is the ice energy, E^{H_2O} is the energy of the isolated H_2O molecules, and N is the number of water molecules. Considering earlier works, several semilocal functionals and their vdW corrected versions have been studied^{92,105,116}. It has been shown that all vdW corrected methods improve considerably the relative energies for the ice phases¹⁰⁵. The results of the PBE, SCAN, TM and revTM functionals for the absolute and relative energies are presented in Table IX, where for the benchmark calculations we used the experimental results and the DMC data taken from Ref.¹⁰⁵.

Inspection of Table IX shows that the revTM performs best for the total sublimation energies (see also Fig. 5), gives the correct ordering of the phases, but overestimates the relative energies with respect to the ice Ih. On the other hand, SCAN significantly underestimates the sublimation energies (see also Fig. 5), but is remarkably

TABLE IX. Sublimation energies per monomer of different phases of ice, computed with various methods. The relative energies of each structure with respect to the ice Ih, are given in parentheses. All energies are in meV/H₂O. Experimental and DMC values from Ref.¹⁰⁵.

	Ih	IX	II	XIII	XIV	XV	VIII
Expt.	-610 (0)	-606 (5)	-609 (1)	—	—	—	-577 (33)
DMC	-605 (0)	—	-609 (-4)	—	—	—	-575 (30)
PBE	-633 (0)	-588 (45)	-564 (69)	-553 (80)	-540 (93)	-523 (110)	-456 (177)
SCAN	-679 (0)	-664 (15)	-670 (9)	-660 (19)	-658 (21)	-652 (27)	-641 (38)
TM	-614 (0)	-621 (-7)	-639 (-25)	-632 (-18)	-635 (-21)	-638 (-24)	-671 (-57)
revTM	-599 (0)	-574 (25)	-575 (24)	-565 (34)	-560 (39)	-554 (45)	-541 (58)

TABLE X. Calculated and experimental equilibrium volumes ($\text{\AA}^3/\text{H}_2\text{O}$) of different phases of ice. The zero-point-energy¹⁰⁶ corrected experimental and DMC values are taken from Ref.¹⁰⁵.

	Ih	IX	II	XIII	XIV	XV	VIII
Expt.	32.05	25.63	24.97	23.91	23.12	22.53	20.09
DMC	31.69	—	24.70	—	—	—	19.46
PBE	30.73	25.74	24.95	24.04	23.20	22.77	20.70
SCAN	29.51	24.19	22.79	21.93	21.21	20.53	18.19
TM	31.18	25.02	23.86	22.72	21.77	21.24	18.41
revTM	31.25	26.03	24.43	23.41	22.65	21.80	19.25

accurate for the relative energies. Here we observe the collapse of the TM meta-GGA, that does not provide the correct ordering of the ice phases, gives negative relative energies, and wrongly predicts the ice VIII as the most stable. In this respect, the performance of revTM is remarkable, correcting all these failures of the TM functional.

The equilibrium volume is another important quantity used to assess the performance of different theoretical methods. Table X shows the equilibrium volumes of the ice phases. We observe that the PBE functional underestimates the ice Ih volume with about 4% (see also Fig. 6) and overestimates the higher density ice VIII with about 3%, otherwise being very accurate (below 1%). Note that the present results of PBE functionals are consistent with the ones of Refs.^{92,105}.

However, for the SCAN and TM meta-GGAs, the tendency is somehow different. Both the SCAN and TM functionals underestimate the equilibrium volume, from lower (Ih phase) to higher (VIII phase) densities. Presumably, this underestimation of the equilibrium volume is because of the presence of a bit much short or intermediate range vdW interaction in the functional form of both of them. We recall that the vdW correction shrinks the volume¹¹⁷. The SCAN and TM functionals underestimate the volume of the ice Ih by about 8% and 3%, and the volume of the ice VIII by about 9% and 8%, respectively (see also Fig. 6). However, the underestimation tendency in volume of the TM functional is greatly modified by revTM due to the de-enhancement of the short-range vdW interaction in the revTM. To encapsulate the behavior of the different functionals, we show in Fig. 6, the relative deviations of the functionals, with respect to the experimental volumes, for several ice phases. PBE and revTM are the most accurate. Note that revTM results have a smaller standard deviation than the PBE

ones.

F. Ice lattice mismatch problem

The impressive performance of the revTM for different ice phases can also endeavor from the popular ice lattice mismatch problem. The lattice mismatch (f) of ice Ih and β -AgI is defined as,

$$f = \frac{2(b-a)}{b+a} \times 100\% , \quad (6)$$

where a and b are the lattice constants of ice Ih and β -AgI respectively.

Practically, f accounts for many applications having industrial uses. For example, it determines the rate of growth of ice on a β -AgI surface. However, computationally one have to get both the lattice constants of ice Ih and β -AgI accurately to obtain the accurate prediction of f . This is quite a difficult task since it involves the simultaneous determination of both the lattice constants of ice Ih and β -AgI having different electronic properties. Most precisely, this is quite a difficult for the semilocal density functionals because it requires to treat both the H-bond (for ice Ih) and strong vdW interactions bond (for β -AgI) within a great accuracy.

In Table XI we summarize the performance of the computed lattice constants of both the materials along with the corresponding lattice mismatch from different methods. Note that the PBE functional was studied previously in several references. For example, in Ref.¹⁹, it was shown that PBE performs better than PBEsol because of its accuracy in the determination of the H-bond. In Ref.¹⁹, it was also shown that the SG4 performs better than PBE and PBEsol. Several meta-GGAs like

TABLE XI. Calculated lattice constants (\AA) for ice Ih and β -AgI as well as the corresponding lattice mismatch as obtained with different functionals. Experimental results are taken from Refs.^{19,116}. The best result for each line is highlighted in bold.

	PBE	SCAN	TM	revTM	Exp.
a (ice Ih)	4.43	4.37	4.45	4.45	4.50
b (β -AgI)	4.69	4.63	4.61	4.61	4.59
mismatch	5.7%	5.8%	3.5%	3.5%	2.2%

revTPSS and MGGA-MS are showing improved performance because of their ability to describe the H-bond¹¹⁶. However, none of these functional are accurate for both the ice Ih and β -AgI simultaneously. From Table XI, we observe that a better balance in the performance is observed for both the ice Ih and β -AgI with the TM and revTM functional. Both perform considerably well and yield a lattice mismatch of 3.5% which is only a 1.3% larger than the experimental values. The SCAN functional performs similarly as the PBE functional with the mismatch of 5.8%. The SCAN functional showing underestimation in the lattice constants of ice Ih. This is probably due to a bit much short or intermediate-range vdW interaction. Note that SCAN, TM, and revTM perform well for the β -AgI. But TM and revTM are more accurate for ice Ih because of their ability to describe the H-bond more accurately. Finally, from the results, we can say that the revTM is a potential candidate for the ice lattice mismatch problem.

G. Merit of performance of TM and revTM functionals

At this point, an elaborating comparison in the performance of the TM and revTM functional from the point of their construction is required. Note that the TM functional includes short or intermediate-range vdW interactions in its exchange due to the oscillation of the exchange enhancement factor originating from the exchange hole model^{38,42,64,118}. However, the revTM functional scales down this short or intermediate-range vdW interactions vdW effects of the TM functional by using a slightly different form of the reduced Laplacian gradient in its exchange functional form⁴². For the general-purpose solids and molecules, this change does not seem to be great consequences except for the dispersion and H-bonded systems for which the short or intermediate-range vdW interaction plays a significant role without including any long-range vdW part. Therefore, we can argue from the present study that, due to this short or intermediate-range vdW interactions, TM functional shows a bit of overestimation tendency in the behavior of the water isomer and cluster which is modified by its revised version i.e, in revTM functional.

For the ice the tendency is quite opposite. In this case inclusion of short or intermediate range vdW interaction actually shriken the volume more. In this sense TM functional shows underestimation in volume which is greatly modified by the change in the exchange enhancement factor of the revTM functional.

IV. CONCLUSIONS

We have studied the performance of TM and revTM functional along with PBE and SCAN functionals for the relative binding energies of the different water hexamer, and dimers. From the present study, we observe that both the SCAN, TM and revTM functional correctly predict the ordering of the stability for different water isomer and cluster. However, the revTM binding energies agree quite well corresponding to the MP2 level theory. Regrading the relative stability of the different water hexamer corresponding to the most state prism structure, the revTM obtains a very accurate result. For neutral, positively, and negatively charged water cluster also, the revTM functional achieves excellent accuracy compared to the PBE, SCAN and TM functionals indicating its accuracy to predict the H-bond in the water cluster. In particular, for water dimer with a single H bond, revTM is consistently giving better absolute binding energies over SCAN. Even for the relative energies for hexamer, the revTM is on an average better than SCAN. This also implies that revTM predicting the short and intermediate-range interactions quite accurately for water. Considering the structural properties of the water monomer, the revTM bit overestimates the results compared to the SCAN functional. Whereas for vibrational frequencies the revTM performs with better accuracy for frequency $\nu < 1000 \text{ cm}^{-1}$. For different ice phases also the revTM shows consistent improvement over the PBE, SCAN and TM functional. It quite accurately predicts the energies and volume of the different ice phases. Also, for the ice lattice mismatch problem the TM and revTM functionals show considerable improved performance over the PBE and SCAN functionals.

In conclusion, the productive power of revTM xc functional showing its great accuracy for different problems which may enables to perform several ab-initio calculations for water useful for physics, chemistry, biological sciences and material physics.

V. SIMULATION DETAILS

We performed calculations of the energetic, structural and vibrational properties of the water isomer and cluster (TABLE II, TABLE III, TABLE IV, TABLE V, TABLE VI, TABLE VII, and TABLE VIII) in the developed version of the Q-CHEM code¹¹⁹ where the XC integrals are calculated with 99 points radial grid and 590 points angular Lebedev grid. The revTM functional results are

compared with the PBE, SCAN, and TM functional. The basis set used for the respective test set are mentioned in headers of each Table.

Details of the HB6, DI6, and CT7 (TABLE I) are collected from previous calculation of ref.⁴², where the 6-311++G(3df,3pd) basis set with NWChem code with the code recommended fine grid are used.

The simulation of the ice phases of water (TABLE IX, TABLE X, and TABLE XI) are calculated using the VASP code¹²⁰ with the hardest projector-augmented wave (PAW) pseudopotentials (H_h and O_h). The 1200 eV energy cutoff and $4 \times 4 \times 4$ \mathbf{k} mesh is used for ice

phases. For water we used a simulation box of volume $20 \times 21 \times 22 \text{ \AA}^3$. We optimize the ice phases using the respective functional to obtain the energies and volume. The calculations of the β -AgI is performed in VASP with the 1200 eV energy cutoff and $16 \times 16 \times 16$ \mathbf{k} Γ -centered \mathbf{k} mesh.

VI. ACKNOWLEDGEMENT

S.J. would like to thank Dr. Biswajit Santra for providing many useful technical informations about the calculation and manuscript.

* subrata.jana@niser.ac.in

† lucian.constantin@iit.it

‡ psamal@niser.ac.in

¹ P. Hohenberg and W. Kohn, Phys. Rev. **136**, B864 (1964).

² J. P. Perdew and A. Zunger, Phys. Rev. B **23**, 5048 (1981).

³ A. D. Becke, Phys. Rev. A **38**, 3098 (1988).

⁴ C. Lee, W. Yang, and R. G. Parr, Phys. Rev. B **37**, 785 (1988).

⁵ J. P. Perdew, J. A. Chevary, S. H. Vosko, K. A. Jackson, M. R. Pederson, D. J. Singh, and C. Fiolhais, Phys. Rev. B **46**, 6671 (1992).

⁶ J. P. Perdew, K. Burke, and M. Ernzerhof, Phys. Rev. Lett. **77**, 3865 (1996).

⁷ E. Fabiano, L. A. Constantin, and F. Della Sala, Phys. Rev. B **82**, 113104 (2010).

⁸ E. Fabiano, L. A. Constantin, and F. Della Sala, J Chem Theory Comput. **7**, 3548 (2011).

⁹ R. Armiento and A. E. Mattsson, Phys. Rev. B **72**, 085108 (2005).

¹⁰ Z. Wu and R. E. Cohen, Phys. Rev. B **73**, 235116 (2006).

¹¹ L. A. Constantin, E. Fabiano, and F. Della Sala, Phys. Rev. B **84**, 233103 (2011).

¹² Y. Zhao and D. G. Truhlar, J. Chem. Phys. **128**, 184109 (2008).

¹³ J. P. Perdew, A. Ruzsinszky, G. I. Csonka, O. A. Vydrov, G. E. Scuseria, L. A. Constantin, X. Zhou, and K. Burke, Phys. Rev. Lett. **100**, 136406 (2008).

¹⁴ L. A. Constantin, A. Terentjevs, F. Della Sala, and E. Fabiano, Phys. Rev. B **91**, 041120 (2015).

¹⁵ L. A. Constantin, J. P. Perdew, and J. M. Pitarke, Phys. Rev. B **79**, 075126 (2009).

¹⁶ L. A. Constantin, L. Chiodo, E. Fabiano, I. Bodrenko, and F. D. Sala, Phys. Rev. B **84**, 045126 (2011).

¹⁷ L. A. Constantin, E. Fabiano, and F. D. Sala, The Journal of Chemical Physics **137**, 194105 (2012).

¹⁸ L. A. Constantin, A. Ruzsinszky, and J. P. Perdew, Phys. Rev. B **80**, 035125 (2009).

¹⁹ L. A. Constantin, A. Terentjevs, F. Della Sala, P. Cortona, and E. Fabiano, Phys. Rev. B **93**, 045126 (2016).

²⁰ A. Cancio, G. P. Chen, B. T. Krull, and K. Burke, J. Chem. Phys. **149**, 084116 (2018).

²¹ L. Chiodo, L. A. Constantin, E. Fabiano, and F. Della Sala, Phys. Rev. Lett. **108**, 126402 (2012).

²² L. A. Constantin, E. Fabiano, S. Laricchia, and F. Della Sala, Phys. Rev. Lett. **106**, 186406 (2011).

²³ A. D. Becke and M. R. Roussel, Phys. Rev. A **39**, 3761 (1989).

²⁴ L. A. Constantin, E. Fabiano, and F. Della Sala, Phys. Rev. B **88**, 125112 (2013).

²⁵ T. Van Voorhis and G. E. Scuseria, J. Chem. Phys. **109**, 400 (1998).

²⁶ Y. Zhao and D. G. Truhlar, J. Chem. Phys. **125**, 194101 (2006).

²⁷ J. P. Perdew, S. Kurth, A. c. v. Zupan, and P. Blaha, Phys. Rev. Lett. **82**, 2544 (1999).

²⁸ J. Tao, J. P. Perdew, V. N. Staroverov, and G. E. Scuseria, Phys. Rev. Lett. **91**, 146401 (2003).

²⁹ J. P. Perdew, A. Ruzsinszky, G. I. Csonka, L. A. Constantin, and J. Sun, Phys. Rev. Lett. **103**, 026403 (2009).

³⁰ L. A. Constantin, E. Fabiano, and F. D. Sala, Phys. Rev. B **86**, 035130 (2012).

³¹ J. P. Perdew, L. A. Constantin, E. Sagvolden, and K. Burke, Phys. Rev. Lett. **97**, 223002 (2006).

³² L. A. Constantin, E. Fabiano, and F. Della Sala, J Chem Theory Comput. **9**, 2256 (2013).

³³ J. Sun, R. Haunschild, B. Xiao, I. W. Bulik, G. E. Scuseria, and J. P. Perdew, J. Chem. Phys. **138**, 044113 (2013).

³⁴ J. Sun, J. P. Perdew, and A. Ruzsinszky, Proc. Natl. Acad. Sci. U. S. A. **112**, 685 (2015).

³⁵ A. Ruzsinszky, J. Sun, B. Xiao, and G. I. Csonka, J Chem Theory Comput. **8**, 2078 (2012).

³⁶ L. A. Constantin, E. Fabiano, J. M. Pitarke, and F. Della Sala, Phys. Rev. B **93**, 115127 (2016).

³⁷ J. Sun, A. Ruzsinszky, and J. P. Perdew, Phys. Rev. Lett. **115**, 036402 (2015).

³⁸ J. Tao and Y. Mo, Phys. Rev. Lett. **117**, 073001 (2016).

³⁹ Y. Wang, X. Jin, H. S. Yu, D. G. Truhlar, and X. He, Proc. Natl. Acad. Sci. U. S. A. **114**, 8487 (2017).

⁴⁰ P. D. Mezei, G. I. Csonka, and M. Kllay, J Chem Theory Comput. **14**, 2469 (2018).

⁴¹ F. Della Sala, E. Fabiano, and L. A. Constantin, Int J Quantum Chem **116**, 1641.

⁴² S. Jana, K. Sharma, and P. Samal, The Journal of Physical Chemistry A **123**, 6356 (2019).

⁴³ B. Patra, S. Jana, L. A. Constantin, and P. Samal, Phys. Rev. B **100**, 045147 (2019).

⁴⁴ A. Patra, S. Jana, H. Myneni, and P. Samal, Phys. Chem. Chem. Phys. , (2019).

⁴⁵ P. Haas, F. Tran, and P. Blaha, Phys. Rev. B **79**, 085104 (2009).

- ⁴⁶ F. Tran, J. Stelzl, and P. Blaha, *J. Chem. Phys.* **144**, 204120 (2016).
- ⁴⁷ Y. Mo, R. Car, V. N. Staroverov, G. E. Scuseria, and J. Tao, *Phys. Rev. B* **95**, 035118 (2017).
- ⁴⁸ A. E. Mattsson, R. Armiento, J. Paier, G. Kresse, J. M. Wills, and T. R. Mattsson, *J. Chem. Phys.* **128**, 084714 (2008).
- ⁴⁹ J. Sun, M. Marsman, G. I. Csonka, A. Ruzsinszky, P. Hao, Y.-S. Kim, G. Kresse, and J. P. Perdew, *Phys. Rev. B* **84**, 035117 (2011).
- ⁵⁰ G. I. Csonka, J. P. Perdew, A. Ruzsinszky, P. H. T. Philipsen, S. Lebègue, J. Paier, O. A. Vydrov, and J. G. Ángyán, *Phys. Rev. B* **79**, 155107 (2009).
- ⁵¹ S. Jana, A. Patra, and P. Samal, *J. Chem. Phys.* **149**, 044120 (2018).
- ⁵² S. Jana, K. Sharma, and P. Samal, *J. Chem. Phys.* **149**, 164703 (2018).
- ⁵³ A. Patra, J. E. Bates, J. Sun, and J. P. Perdew, *Proc. Natl. Acad. Sci. U. S. A.* **114**, E9188 (2017).
- ⁵⁴ J. Sun, B. Xiao, Y. Fang, R. Haunschild, P. Hao, A. Ruzsinszky, G. I. Csonka, G. E. Scuseria, and J. P. Perdew, *Phys. Rev. Lett.* **111**, 106401 (2013).
- ⁵⁵ H. Peng, Z.-H. Yang, J. P. Perdew, and J. Sun, *Phys. Rev. X* **6**, 041005 (2016).
- ⁵⁶ C. J. Cramer and D. G. Truhlar, *Phys. Chem. Chem. Phys.* **11**, 10757 (2009).
- ⁵⁷ R. Peverati and D. G. Truhlar, *Philos. Trans. R. Soc., A* **372** (2014), 10.1098/rsta.2012.0476.
- ⁵⁸ L. A. Curtiss, K. Raghavachari, G. W. Trucks, and J. A. Pople, *J. Chem. Phys.* **94**, 7221 (1991).
- ⁵⁹ V. N. Staroverov, G. E. Scuseria, J. Tao, and J. P. Perdew, *J. Chem. Phys.* **119**, 12129 (2003).
- ⁶⁰ Y. Zhao, N. E. Schultz, and D. G. Truhlar, *J Chem Theory Comput.* **2**, 364 (2006).
- ⁶¹ L. Goerigk and S. Grimme, *J Chem Theory Comput.* **7**, 291 (2011).
- ⁶² P. Hao, J. Sun, B. Xiao, A. Ruzsinszky, G. I. Csonka, J. Tao, S. Glindmeyer, and J. P. Perdew, *J Chem Theory Comput.* **9**, 355 (2013).
- ⁶³ L. Goerigk, A. Hansen, C. Bauer, S. Ehrlich, A. Najibi, and S. Grimme, *Phys. Chem. Chem. Phys.* **19**, 32184 (2017).
- ⁶⁴ Y. Mo, G. Tian, R. Car, V. N. Staroverov, G. E. Scuseria, and J. Tao, *J. Chem. Phys.* **145**, 234306 (2016).
- ⁶⁵ Y. Mo, G. Tian, and J. Tao, *Phys. Chem. Chem. Phys.* **19**, 21707 (2017).
- ⁶⁶ S. Grimme, *Wiley Interdisciplinary Reviews: Computational Molecular Science* **1**, 211 (2011).
- ⁶⁷ A. Tkatchenko, R. A. DiStasio, R. Car, and M. Scheffler, *Phys. Rev. Lett.* **108**, 236402 (2012).
- ⁶⁸ M. J. Gillan, D. Alf, and A. Michaelides, *The Journal of Chemical Physics* **144**, 130901 (2016).
- ⁶⁹ B. Santra, A. Michaelides, and M. Scheffler, *The Journal of Chemical Physics* **127**, 184104 (2007).
- ⁷⁰ R. A. DiStasio, B. Santra, Z. Li, X. Wu, and R. Car, *The Journal of Chemical Physics* **141**, 084502 (2014).
- ⁷¹ M. Chen, H.-Y. Ko, R. C. Remsing, M. F. Calegari Andrade, B. Santra, Z. Sun, A. Selloni, R. Car, M. L. Klein, J. P. Perdew, and X. Wu, *Proceedings of the National Academy of Sciences* **114**, 10846 (2017).
- ⁷² L. Zheng, M. Chen, Z. Sun, H.-Y. Ko, B. Santra, P. Dhuvad, and X. Wu, *The Journal of Chemical Physics* **148**, 164505 (2018).
- ⁷³ J. C. Grossman, E. Schwegler, E. W. Draeger, F. Gygi, and G. Galli, *The Journal of Chemical Physics* **120**, 300 (2004), <https://doi.org/10.1063/1.1630560>.
- ⁷⁴ E. Schwegler, J. C. Grossman, F. Gygi, and G. Galli, *The Journal of Chemical Physics* **121**, 5400 (2004), <https://doi.org/10.1063/1.1782074>.
- ⁷⁵ D. A. Estrin, L. Paglieri, G. Corongiu, and E. Clementi, *The Journal of Physical Chemistry* **100**, 8701 (1996).
- ⁷⁶ P. N. Day, R. Pachter, M. S. Gordon, and G. N. Merrill, *The Journal of Chemical Physics* **112**, 2063 (2000).
- ⁷⁷ H. M. Lee, S. B. Suh, J. Y. Lee, P. Tarakeshwar, and K. S. Kim, *The Journal of Chemical Physics* **112**, 9759 (2000).
- ⁷⁸ C. Zhang, J. Wu, G. Galli, and F. Gygi, *Journal of Chemical Theory and Computation* **7**, 3054 (2011).
- ⁷⁹ R. Bader and T. Nguyen-Dang, in *Advances in Quantum Chemistry*, Vol. 14 (Elsevier, 1981) pp. 63–124.
- ⁸⁰ A. Becke, *The quantum theory of atoms in molecules: from solid state to DNA and drug design* (John Wiley & Sons, 2007).
- ⁸¹ S. J. Grabowski, *The Journal of Physical Chemistry A* **105**, 10739 (2001).
- ⁸² J. Contreras-García, W. Yang, and E. R. Johnson, *The Journal of Physical Chemistry A* **115**, 12983 (2011).
- ⁸³ E. Fabiano, L. Constantin, and F. Della Sala, *Journal of chemical theory and computation* **10**, 3151 (2014).
- ⁸⁴ C. Tsai and K. Jordan, *Chemical Physics Letters* **213**, 181 (1993).
- ⁸⁵ K. Laasonen, M. Parrinello, R. Car, C. Lee, and D. Vanderbilt, *Chemical Physics Letters* **207**, 208 (1993).
- ⁸⁶ R. M. Olson, J. L. Bentz, R. A. Kendall, M. W. Schmidt, and M. S. Gordon, *Journal of Chemical Theory and Computation* **3**, 1312 (2007).
- ⁸⁷ T. Todorova, A. P. Seitsonen, J. Hutter, I.-F. W. Kuo, and C. J. Mundy, *The Journal of Physical Chemistry B* **110**, 3685 (2006), pMID: 16494424, <https://doi.org/10.1021/jp055127v>.
- ⁸⁸ M. V. Fernández-Serra and E. Artacho, *The Journal of Chemical Physics* **121**, 11136 (2004), <https://aip.scitation.org/doi/pdf/10.1063/1.1813431>.
- ⁸⁹ H.-S. Lee and M. E. Tuckerman, *The Journal of Physical Chemistry A* **110**, 5549 (2006), pMID: 16623489, <https://doi.org/10.1021/jp0570770>.
- ⁹⁰ C. Lee, D. Vanderbilt, K. Laasonen, R. Car, and M. Parrinello, *Phys. Rev. Lett.* **69**, 462 (1992).
- ⁹¹ B. Militzer and H. F. Wilson, *Phys. Rev. Lett.* **105**, 195701 (2010).
- ⁹² B. Santra, J. c. v. Klimeš, D. Alfè, A. Tkatchenko, B. Slater, A. Michaelides, R. Car, and M. Scheffler, *Phys. Rev. Lett.* **107**, 185701 (2011).
- ⁹³ B. Santra, A. Michaelides, M. Fuchs, A. Tkatchenko, C. Filippi, and M. Scheffler, *The Journal of Chemical Physics* **129**, 194111 (2008).
- ⁹⁴ E. E. Dahlke, R. M. Olson, H. R. Leverentz, and D. G. Truhlar, *The Journal of Physical Chemistry A* **112**, 3976 (2008).
- ⁹⁵ D. M. Bates and G. S. Tschumper, *The Journal of Physical Chemistry A* **113**, 3555 (2009).
- ⁹⁶ A. Otero-de-la Roza and E. R. Johnson, *The Journal of Chemical Physics* **138**, 204109 (2013).
- ⁹⁷ Y. Chen and H. Li, *The Journal of Physical Chemistry A* **114**, 11719 (2010).

- ⁹⁸ J. Sun, R. C. Remsing, Y. Zhang, Z. Sun, A. Ruzsinszky, H. Peng, Z. Yang, A. Paul, U. Waghmare, X. Wu, M. L. Klein, and J. P. Perdew, *Nature Chemistry* **8**, 831 EP (2016), article.
- ⁹⁹ J. P. Perdew, J. Tao, V. N. Staroverov, and G. E. Scuseria, *J. Chem. Phys.* **120**, 6898 (2004).
- ¹⁰⁰ Y. Zhao and D. G. Truhlar, *J. Chem. Theory Comput.* **3**, 289 (2007).
- ¹⁰¹ B. Temelso, K. A. Archer, and G. C. Shields, *The Journal of Physical Chemistry A* **115**, 12034 (2011).
- ¹⁰² D. Manna, M. K. Kesharwani, N. Sylvetsky, and J. M. Martin, *Journal of chemical theory and computation* **13**, 3136 (2017).
- ¹⁰³ C. Gray and K. Gubbins, *Theory of Molecular Fluids: Vol. 1: Fundamentals* (Clarendon Press, 1984).
- ¹⁰⁴ S. Jana, L. Constantin, and P. Samal, Supporting Information.
- ¹⁰⁵ B. Santra, J. Klime, A. Tkatchenko, D. Alf, B. Slater, A. Michaelides, R. Car, and M. Scheffler, *The Journal of Chemical Physics* **139**, 154702 (2013), <https://doi.org/10.1063/1.4824481>.
- ¹⁰⁶ S. Rasti and J. Meyer, *The Journal of chemical physics* **150**, 234504 (2019).
- ¹⁰⁷ S. S. Xantheas, C. J. Burnham, and R. J. Harrison, *The Journal of Chemical Physics* **116**, 1493 (2002).
- ¹⁰⁸ G. S. Fanourgakis, E. Apr, W. A. de Jong, and S. S. Xantheas, *The Journal of Chemical Physics* **122**, 134304 (2005).
- ¹⁰⁹ M. E. Dunn, T. M. Evans, K. N. Kirschner, and G. C. Shields, *The Journal of Physical Chemistry A* **110**, 303 (2006).
- ¹¹⁰ J. Xu, M. Chen, C. Zhang, and X. Wu, *Phys. Rev. B* **99**, 205123 (2019).
- ¹¹¹ J. Wiktor, F. Ambrosio, and A. Pasquarello, *The Journal of Chemical Physics* **147**, 216101 (2017).
- ¹¹² J. C. Howard, J. L. Gray, A. J. Hardwick, L. T. Nguyen, and G. S. Tschumper, *Journal of Chemical Theory and Computation* **10**, 5426 (2014).
- ¹¹³ J. C. Howard and G. S. Tschumper, *Journal of Chemical Theory and Computation* **11**, 2126 (2015).
- ¹¹⁴ C. G. Salzmann, P. G. Radaelli, B. Slater, and J. L. Finney, *Phys. Chem. Chem. Phys.* **13**, 18468 (2011).
- ¹¹⁵ C. G. Salzmann, P. G. Radaelli, E. Mayer, and J. L. Finney, *Phys. Rev. Lett.* **103**, 105701 (2009).
- ¹¹⁶ Y. Fang, B. Xiao, J. Tao, J. Sun, and J. P. Perdew, *Phys. Rev. B* **87**, 214101 (2013).
- ¹¹⁷ A. V. Terentjev, L. A. Constantin, and J. M. Pitarke, *Phys. Rev. B* **98**, 214108 (2018).
- ¹¹⁸ H. Tang and J. Tao, *Materials Research Express* **5**, 076302 (2018).
- ¹¹⁹ Y. Shao, Z. Gan, E. Epifanovsky, A. T. Gilbert, M. Wormit, J. Kussmann, A. W. Lange, A. Behn, J. Deng, X. Feng, D. Ghosh, M. Goldey, P. R. Horn, L. D. Jacobson, I. Kaliman, R. Z. Khaliullin, T. Ku, A. Landau, J. Liu, E. I. Proynov, Y. M. Rhee, R. M. Richard, M. A. Rohrdanz, R. P. Steele, E. J. Sundstrom, H. L. W. III, P. M. Zimmerman, D. Zuev, B. Albrecht, E. Alguire, B. Austin, G. J. O. Beran, Y. A. Bernard, E. Berquist, K. Brandhorst, K. B. Bravaya, S. T. Brown, D. Casanova, C.-M. Chang, Y. Chen, S. H. Chien, K. D. Closser, D. L. Crittenden, M. Diedenhofen, R. A. D. Jr., H. Do, A. D. Dutoi, R. G. Edgar, S. Fatehi, L. Fusti-Molnar, A. Ghysels, A. Golubeva-Zadorozhnaya, J. Gomes, M. W. Hanson-Heine, P. H. Harbach, A. W. Hauser, E. G. Hohenstein, Z. C. Holden, T.-C. Jagau, H. Ji, B. Kaduk, K. Khistyayev, J. Kim, J. Kim, R. A. King, P. Klunzinger, D. Kosenkov, T. Kowalczyk, C. M. Krauter, K. U. Lao, A. D. Laurent, K. V. Lawler, S. V. Levchenko, C. Y. Lin, F. Liu, E. Livshits, R. C. Lochan, A. Luenser, P. Manohar, S. F. Manzer, S.-P. Mao, N. Mardirossian, A. V. Marenich, S. A. Maurer, N. J. Mayhall, E. Neuscamman, C. M. Oana, R. Olivares-Amaya, D. P. O'Neill, J. A. Parkhill, T. M. Perrine, R. Peverati, A. Prociuk, D. R. Rehn, E. Rosta, N. J. Russ, S. M. Sharada, S. Sharma, D. W. Small, A. Sodt, T. Stein, D. Stck, Y.-C. Su, A. J. Thom, T. Tsuchimochi, V. Vanovschi, L. Vogt, O. Vydrov, T. Wang, M. A. Watson, J. Wenzel, A. White, C. F. Williams, J. Yang, S. Yeganeh, S. R. Yost, Z.-Q. You, I. Y. Zhang, X. Zhang, Y. Zhao, B. R. Brooks, G. K. Chan, D. M. Chipman, C. J. Cramer, W. A. G. III, M. S. Gordon, W. J. Hehre, A. Klamt, H. F. S. III, M. W. Schmidt, C. D. Sherrill, D. G. Truhlar, A. Warshel, X. Xu, A. Aspuru-Guzik, R. Baer, A. T. Bell, N. A. Besley, J.-D. Chai, A. Dreuw, B. D. Dunietz, T. R. Furlani, S. R. Gwaltney, C.-P. Hsu, Y. Jung, J. Kong, D. S. Lambrecht, W. Liang, C. Ochsenfeld, V. A. Rassolov, L. V. Slipchenko, J. E. Subotnik, T. V. Voorhis, J. M. Herbert, A. I. Krylov, P. M. Gill, and M. Head-Gordon, *Molecular Physics* **113**, 184 (2015).
- ¹²⁰ G. Kresse and J. Hafner, *Phys. Rev. B* **47**, 558 (1993).